Micrometric drilling of (meta-)studtite square platelets formed by pseudomorphic conversion of UO2 under high-frequency ultrasound

Julien Margate, Matthieu Virot, Thomas Dumas, Christophe Jégou, Tony Chave, Manon Cot-Auriol, Ange Alves, Sergey Nikitenko

Micrometric drilling of (meta-)studtite square platelets formed by pseudomorphic conversion of UO_2 under high-frequency ultrasound

Julien Margate,[1] Matthieu Virot,[1*] Thomas Dumas,[2] Christophe Jégou,[3] Tony Chave[1], Manon Cot-Auriol,[1] Ange Alves,[1] Sergey I. Nikitenko[1]

[1] ICSM, Univ Montpellier, CEA, CNRS, ENSCM, Marcoule, France.
[2] CEA, DES, ISEC, DMRC, Univ Montpellier, Marcoule, France.
[3] CEA, DES, ISEC, DPME, Univ Montpellier, Marcoule, France.
* matthieu.virot@cea.fr

Abstract

Pseudomorphic transformations are related to chemical conversions of materials while conserving their shape and structural features. Structuring ceramic shapes this way can be used to tailor the physico-chemical properties of materials that can benefit particular applications. In the context of spent nuclear fuel storage interacting with radiolysis products, the sonochemical behavior of powdered UO_2 was investigated in dilute aqueous solutions saturated with Ar/(20%)O_2 (20 °C). Optimized parameter settings enabled the complete conversion of UO_2 micrometric platelets into uranyl peroxide precipitates, referred to as (meta-)studtite [$(UO_2(O_2)(H_2O)_2)\cdot xH_2O$] with x = 2 or 4. While the most acidic conditions yielded elongated crystal shapes in agreement with a dissolution/reprecipitation mechanism, softer conditions allowed the pseudomorphic transformation of the platelet shape oxide suggesting a complex formation mechanism. For specific conditions, this unprecedented morphology was accompanied with the formation of a hole in the platelet center. Investigations revealed that the formation of the drilled polymorphs is related to a perfect blend of H^+, *in-situ* generation of H_2O_2 and high-frequency ultrasound, and is most probably related to the sono-capillary effect. These insights pave the way for new sonochemical approaches dedicated to the preparation of material polymorphs tailoring specific structural properties.

Environmental implication

Radioactive uranium oxide (UO_2) plays a central role for current and future nuclear energetics. A comprehensive knowledge about its behaviour in the presence of hydrogen peroxide is of paramount interest in order to understand its fate in storage conditions and the highly questioned environmental migration schemes. Assessing the precipitation processes for uranium-based peroxides in relation to the morphology of the precipitates and the physicochemical formation conditions remains an important issue. The physical and chemical effects driven by the acoustic cavitation phenomenon offer a promising alternative for nuclear chemistry studies including the in-situ generation of H_2O_2 as an alternative to radiolysis.

1. Introduction

Understanding the mechanisms of uranium peroxides formation is of prime importance as these compounds are involved both in the front-end and back-end of the nuclear fuel cycle. Assessing the peroxide precipitation processes in relation to the morphology of the precipitates and the conditions responsible for their formation remains an important issue. In many established scenarios (failure of irradiated fuel rods in storage pool, deep geological disposal, nuclear accident, etc.),[1–3] uranium peroxide formation may particularly occur as a result of the corrosion and alteration of spent uranium dioxide nuclear fuels made up of about 95 wt% of UO_2 and 5 wt% of fission products and transuranic elements.[4] The formation of these secondary phases is highly dependent upon the surrounding conditions and the nature of the involved reactive species. The formation of uranium oxides or hydrated uranyl oxides arising from UO_2 oxidative behavior has been extensively studied[5,6] and is discussed in a review by Shoesmith.[7] Due to the radioactive materials contained in the storage matrix, several chemically reactive species can be formed as a result of water radiolysis: e^-_{aq}, H^+, H_2 and HO^-, $HO^\bullet$ and H_2O_2. The latter has been demonstrated to be one of the most important generated reactants, even in anoxic conditions.[1,8,9] In disposal conditions, the generation of oxidants may contribute in the oxidation of U(IV) to U(VI) and slow corrosion of the UO_2 matrix.[4,7,10]

In natural conditions, studtite $[(UO_2(O_2)(H_2O)_2)\cdot 2H_2O]$ and metastudtite $[(UO_2(O_2)(H_2O)_2]$, are the only peroxide minerals that have been reported. The structure of studtite has been resolved by Burns et al. and the one of meta-studtite was proposed by Weck et al. using density functional theory.[11,12] Studtite, is an uranyl peroxide that can lose water molecules in air-conditions to form metastudtite, it contains $U(VI)O_2^{2+}$ cations bonded with 4 oxygen atoms from peroxide groups and 2 from water molecules that polymerize into chains sharing peroxide groups. Both phases can be obtained depending on the experimental conditions. Some authors reported the formation of studtite[13,14] while others obtained metastudtite.[4] Additionally, a change in the uranyl covalence during dehydration has been reported using spectroscopic and theoretical methods.[15] Nevertheless, some structural variations can be easily identified according to XRD and Raman spectroscopy in order to distinguish both phases.[16]

Since the early 90s', many studies have focused on the oxidative dissolution of UO_2 by H_2O_2 under different conditions (e.g. presence of CO_3^{2-}, Ca^{2+}, SiO_4^-) and the slow formation of hyperstoichiometric uranium oxides (UO_{2+x}) on the surface of the starting oxide was particularly reported.[5,7,14,17–19] Studies focusing the evolution of the concentration of uranium produced from UO_2 dissolution with H_2O_2 in aqueous solution evidenced the formation of secondary phases attributed to studtite.[13,20,21] Several mechanisms have been proposed to understand the impact of aqueous radiolytic oxidants on the dissolution of UO_2. H_2O_2 can be catalytically decomposed on oxide surfaces into O_2 and H_2O in aqueous solution with the formation of hydroxyl radicals bound to the surface. **(Eq. 1-3)**[22,23] or it can play a major role in the oxidative dissolution of UO_2-based material leading to the matrix dissolution described by **(Eq. 4-7)**.[18,19,24,25]

E. Ekeroth et al. have described the oxidation step as the limiting step in the conversion of UO_2 to uranyl peroxide.[24] In a system containing UO_2 and H_2O_2, Pablo et al. demonstrated that the consumption of H_2O_2 is faster than the dissolution of UO_2.[13] The authors concluded that this observation results from the formation of oxidized products of uranium that remains on the solid surface. Using atomic force microscopy, they also characterized the formation of uranyl peroxide structure found on UO_2 surface. In the literature, some detailed mechanisms about surface oxidation have also been proposed in aqueous solution in order to explain the formation of peroxo-species. [18,26,27]

$$H_2O_2 \rightarrow 2\ HO^{\bullet} \qquad \textbf{Eq. 1}$$
$$HO^{\bullet} + H_2O_2 \rightarrow HO_2^{\bullet} + H_2O \qquad \textbf{Eq. 2}$$
$$HO_2^{\bullet} + HO_2^{\bullet} \rightarrow H_2O_2 + O_2 \qquad \textbf{Eq. 3}$$

$$½\ H_2O_2 + UO_{2(s)} \rightarrow UO_{2(s)}\text{--}HO^{\bullet} \qquad \textbf{Eq. 4}$$
$$H_2O_2 + UO_{2(s)}\text{--}HO^{\bullet} \rightarrow HO_2^{\bullet} + UO_2 + H_2O \qquad \textbf{Eq. 5}$$
$$UO_{2(s)}\text{--}HO^{\bullet} \rightarrow HO^{-} + UO_2^{+}{}_{(s)} \qquad \textbf{Eq. 6}$$
$$UO_2^{+}{}_{(s)} + UO_2^{+}{}_{(s)} \rightarrow UO_2^{2+}{}_{(aq)} + UO_{2(s)} \qquad \textbf{Eq. 7}$$

Sonochemistry, which deals with the effect of ultrasonic waves on chemical reactions, has proven to be an innovative approach for the study of homogeneous and heterogeneous solid/liquid systems that considered actinides.[28–30] It also remains an interesting and an original way to simulate the products of water radiolysis under alpha and beta gamma irradiation. The observed effects are attributed to the acoustic cavitation phenomenon, which gathers the successive nucleation, growth and rapid implosion of gas and vapour-filled microbubbles. At the final stage of collapse, plasma-chemical conditions have been demonstrated to be at the origin of the formation of excited species and radicals. Hence, H_2O_2 is known to accumulate in aqueous solutions (and H_2 in the gas phase) submitted to ultrasound as a result of water molecule splitting **(Eq. 8-9)**.[31–33]

$$H_2O \rightarrow))) \rightarrow HO^{\bullet} + H^{\bullet} \qquad \textbf{Eq. 8}$$
$$HO^{\bullet} + HO^{\bullet} \rightarrow H_2O_2 \qquad \textbf{Eq. 9}$$

$$O_2 + H^{\bullet} \rightarrow HO_2^{\bullet} \qquad \textbf{Eq. 10}$$
$$HO_2^{\bullet} + HO_2^{\bullet} \rightarrow H_2O_2 + O_2 \qquad \textbf{Eq. 11}$$

Under oxygenated argon atmosphere (*e.g.* Ar/(20%)O_2) the quantity of H_2O_2 produced increases dramatically due to the scavenging of $H^{\bullet}$ radicals by the dioxygen molecules **(Eq. 10)**. This reaction prevents the recombination of the $H^{\bullet}$ and $HO^{\bullet}$ radicals formed by the reaction **Eq. 8** and enable the production of hydroperoxyl radicals, regenerating O_2 and accumulating H_2O_2 **(Eq. 11)**. At high ultrasonic frequency (100 kHz-1 MHz), H_2O_2 formation rate can be dramatically enhanced compared to 20 kHz ultrasound due to the dissociation of O_2 molecules inside the acoustic bubbles.[34] In addition to the above reported chemical effects, the implosion of the cavitation bubbles generated by low-frequency ultrasound (20-40 kHz) causes the propagation of spherical shock waves that can significantly affect solid materials. When imploding at the vicinity of an extended solid surface, a micro-jet of liquid

directed towards the surface with a high velocity may form (ca. 150 $m.s^{-1}$ at 20 kHz). [35] Several effects have been reported in consequence including surface cleaning, depassivation, particle dispersion and fragmentation, etc. [29,36,37] The combined physical and chemical effects driven by the acoustic cavitation phenomenon are therefore promising for nuclear chemistry studies. Sonochemistry has been already applied for the dissolution or activation of refractory actinide materials including for instance UC, UO_3, UO_2, ThO_2 or PuO_2.[38,39] Particularly, 20 kHz sonication of ThO_2 in dilute sulphuric medium saturated with $Ar/(20\%)O_2$ recently led to its significant dissolution and partial conversion into a Th(IV) peroxide compound which structure was later resolved.[40,41]

In the present work, the sonochemical behaviour of UO_2 and its conversion into uranyl peroxide was investigated in pure water and dilute aqueous solutions of H_2SO_4. The pH remains a key parameter involved in the speciation of uranium and the precipitation of peroxides. Continuous monitoring of the solution allowed to follow the dissolution of uranium dioxide and the accumulation/consumption of hydrogen peroxide. Further analyses of the solid residues led to new questions about the behaviour of UO_2 in aqueous solution with respect to the sonochemical conditions that significantly affected the morphology of the as-formed uranyl peroxides. In particular, optimized conditions enabled the polymorphic transformation of uranyl peroxides showing an unprecedented morphology which formation mechanism was deciphered.

2. Experimentals

Solutions were prepared with Milli-Q water having a resistivity higher than 18.2 MΩ.cm at 25°C. The various reagents used in this work were all of analytical grade and purchased from Sigma Aldrich. Uranium metal were supplied by CETAMA. The experiments were performed under an Ar/(20%)O_2 gas mixture provided by Air Liquide.

2.1. UO_2 synthesis

UO_2 was synthesized using the oxalic route. Briefly, uranium metal was dissolved in 6 M HCl and stabilized at the tetravalent state U(IV) in 1 M HCl solution before being added dropwise to a solution of oxalic acid under strong agitation. After 1 h, the obtained precipitate was centrifuged and washed three times with pure water before being dried overnight under Ar flow. This oxalate precursor was then fired at 485 °C (4 h) or 800 °C (2 h) in a reducing atmosphere Ar/(4%)H_2 with a 1 h step at 100 °C.[42] The obtained oxide powders were characterized by Powder X-ray Diffraction (PXRD) and Scanning Electron Microscopy (SEM) which evidenced the preparation of UO_2 exhibiting a typical square plate morphology (**Fig. S1** and **S2**, **ESI**).[42]

2.2. Sonochemical experiments

Low frequency (20 kHz) ultrasonic treatment was performed in a 50 mL thermostated batch reactor equipped with a cooling system and a main central opening. The latter allows maintaining the titanium-based sonotrode (tip of 1 cm^2) with a PTFE seal. The power supply was provided by a 750 W generator (Sonics & materials Vibracell VCX 750) used at a 30% amplitude involving an acoustic power of 0.36 $W{\cdot}mL^{-1}$. For 346 and 1046 kHz, ultrasonic treatments were performed in a cylindrical reactor of 250 mL mounted on top of 25 cm^2 high-frequency transducers (L3 communication ELAC Nautik) connected to a 125 W generator (LVG 60 RF-generator). A mechanical stirring of 300 rpm was applied during high frequency sonolyses to obtain a homogeneous system. For 100 and 550 kHz frequency ultrasound, the cylindrical reactor was mounted on top of stainless-steel transducers purchased from SinapTec (France). Transducers were connected to a generator (SinapTec Lab500) having a maximum electrical power of 120 W for 100 kHz and 100 W for 550 kHz. Both high and low frequency reactors were equipped with side inlets for the temperature control, the circulation of a bubbling gas and sample collections. The temperature inside both reactors was maintained at 20 °C during ultrasonic treatment using a cryostat (Lauda Eco RE 1050) and a thermocouple immersed in the solution.

For all of the sonication experiments, the power (W) delivered to the solution was estimated by the calorimetric method.[43] The calculated acoustic power ($W.mL^{-1}$) was then determined through normalization by taking into account the sonicated volume of the solution. Typical experiments involved the sonication of 200 mg of UO_2 powder dispersed in 50 mL (20 kHz) or 250 mL (100 kHz – 1 MHz) of pure water or dilute sulfuric acid (100 kHz – 1 MHz). The pH of the solutions before sonication was pH= 5.5 for pure water, pH= 2.2 for 0.5 M H_2SO_4 and pH= 3.2 for 0.05 M H_2SO_4. Control experiments were carried out under similar conditions without ultrasound. The potential presence of carbonates in the sonicated dispersions was rejected before and after sonication using a Shimadzu COT-meter which revealed a concentration below 3 ppm. During ultrasound exposure, the evolution of the reaction media was characterized after filtration on 0.2 µm PTFE filters by ICP/AES and UV-

Visible absorption spectroscopy. Solution aliquots were also centrifuged to characterize the solid phase evolution (after several washing with pure water) with SEM, AFM and PXRD.

2.3. Analyses and characterizations

UV-visible absorption spectroscopy

During the experiments, solution aliquots (1 mL) were regularly sampled from the reactor, filtered with 0.2 µm PTFE filters and dilute with a Ti(IV) solution for analysis with UV–Vis absorption spectroscopy to follow H_2O_2 formation rates (Thermo Evolution 220, Thermo scientific). The addition of the Ti(IV) solution allows the formation of a Ti(IV)-H_2O_2 complex absorbing at 410 nm[44] which allowed to deduce the concentration of H_2O_2 in solution using the Beer-Lambert law. Absorption spectra were measured in a 1 cm quartz cell from 300 to 750 nm. The Ti(IV) solution was prepared by dissolving 0.322 g of $TiOSO_4$ (2.10^{-2} M) in 0.5 M H_2SO_4 under stirring and gentle heating. A calibration curve was previously prepared with a standard H_2O_2 solution to determine the molar extinction coefficient of the complex (ε= 721.4 $L{\cdot}cm^{-1}{\cdot}mol^{-1}$ at λ_{max} = 410 nm). Statistical error is estimated to 10%.

Inductively coupled plasma-optical emission spectroscopy (ICP-OES)

The concentration of selected elements in solution over time was determined using an ICAP 7000 series model (Thermo Scientific). Samples were prepared by diluting solution aliquots in a 0.3 M HNO_3 solution. The concentrations of the target elements were obtained against an external calibration curve prepared with standards (SCP Science) between 0.5 and 15 $mg{\cdot}L^{-1}$. Results obtained at λ = 385.958 nm for uranium were considered. The UO_2 dissolution rate was estimated with statistical error lower than 10%.

Powder X-ray diffraction (PXRD)

PXRD diagrams were acquired using a Bruker D8 Advance X-Ray diffractometer equipped with a linear Lynx-eye detector (Cu $K\alpha_{1,2}$ radiation, λ = 1.51184 Å). The data were collected at room temperature with a 2θ value ranging between 5° and 120°, a step of 0.019° and a counting time of 1.78 s per step. The samples were deposited on a low background support with a drop of absolute ethanol and confined in a dome to avoid the potential contamination of the surroundings. The diffraction patterns were identified with the International Centre for Diffraction Data database (ICDD) using DIFFRAC.EVA software (Bruker, Germany). GSAS-II software was used to discriminate the proportion of U_3O_8, UO_2 and peroxides phases in the pattern.

Scanning electron microscopy (SEM)

SEM was used to study the morphology evolution of the solids during ultrasonic treatment using a FEI Quanta 200 ESEM FEG electron microscope or with a FEI Helios 600 Nanolab dual beam. The samples were deposited onto carbon tapes and analysed without any specific preparation. The 3D reconstruction images were made with Alicona MeX V5.1 software using tilted images acquired by SEM as described previously.[45]

Focused Ion Beam-Scanning Electron Microscopy (FIB-SEM)

An ultrafine lamellae of our samples was obtained with a focused ion beam (FIB), FEI Helios 600 Nanolab (CP2M, Marseille, France). After SiO and Pt deposit layers, thin micrometer sections were lifted in situ and transferred onto a half-copper grid using an Omniprobe 200

micromanipulator up to electron transparency (final thickness of about 100 nm). This cutting process took place at a reduced acceleration voltage of 5 kV to reduce beam damage.

Transmission electron microscopy (TEM)

FIB lamella was analyzed by transmission electron microscopy TEM on FEI Tecnaï G2 with a LaB_6 source operating at 200 kV equipped with a CCD TVIPS 1k*1k camera.

Atomic Force Microscopy (AFM)

UO_2 sample morphologies were studied by AFM using a MULTIMODE 8 AFM device supplied with Nanoscope 5 software from Bruker (Germany). Typically, droplets of solid residues dispersed in absolute ethanol were deposited onto Cu disk. The images were acquired in tapping mode (2 khz) using SNL tips (k= 0.35 N/m)

CHESS (Chemical Equilibrium of Species and Surfaces) code

CHESS code developed by the Ecole des Mines de Paris was used to calculate chemical speciation in aqueous solution. Computation was performed at thermodynamic equilibrium using CHESS v3.0 and the EQ3/6 database.[46]

3. Results

3.1. Sonochemical conversion of UO_2 into uranyl peroxides

Fig. 1.a displays the dissolution kinetics of uranium in pure water and sulfuric media observed during the 346 kHz sonication of UO_2 fired at 800°C. **Fig. 1.b** illustrates the corresponding sonochemical kinetics related to the accumulation of H_2O_2 in solution. The accumulation rates for uranium was found higher in acidic media than in pure water with similar sonochemical conditions. The highest dissolution rate was observed in concentrated 5 mM H_2SO_4 medium (**Fig 1.a**). Some authors reported an increase of UO_2 dissolution in aqueous solution when decreasing the pH in agreement with the reaction **Eq. 12.**[21,47] For a H_2O_2 concentration of ca. 10^{-3} M, Clarens et al. stated that the dissolution rate does not depend on the pH in the acidic range and attributed this difference to the precipitation of an uranium solid phase (uranyl peroxide, **Eq. 13**).[48] Such a behavior could explain the shape of the accumulation curve observed for uranium in the 5 mM H_2SO_4 aqueous solution.

$$H_2O_2 + UO_2 + 2\ H^+ \rightarrow 2\ H_2O + UO_2^{2+} \qquad \textbf{Eq. 12}$$

$$UO_2^{2+} + H_2O_2 + xH_2O \rightarrow UO_2(O_2)\cdot xH_2O(s) + 2\ H^+ \qquad \textbf{Eq. 13}$$

Whatever the medium, sonochemical accumulation rates of H_2O_2 observed in the presence of UO_2 powder were found lower than the reference experiment carried out without solid (**Fig. 1.b**). **Table 1** compares H_2O_2 formation yields for the various systems, which agree with these observations and also suggest a higher consumption of H_2O_2 in acidic conditions. In agreement with the literature, the differences observed in these conditions can originate three processes: oxidation of U(IV) into U(VI), precipitation of secondary phases, catalytic decomposition of H_2O_2 at UO_2 surface.[7] Generally, the pH observed for our experiments carried out in acidic conditions was stable (pH = 2.2 for 5 mM H_2SO_4 and pH = 3.2 for 0.5 mM H_2SO_4), whereas it significantly decreased during sonolysis in pure water (ranging from 5.8 to 3.7). Such a pH decrease can be attributed to the possible surface hydrolysis of UO_2 that may be promoted under ultrasound irradiation.[49,50] In the global conversion process (**Eq. 12-13**), protons play the role of a catalyst. Note that for similar other conditions carried out in the absence of ultrasound but with addition of H_2O_2, the pH of the solution only decreased from 5.8 to 5.4 during 6 h experiments evidencing the dramatic effect of the acoustic cavitation and *in-situ* generation of hydrogen peroxide. Furthermore, the colour of the sonicated suspension became lighter during the experiment indicating the significant modification of the solid phase **(Fig. S3)**.

Table 1: H_2O_2 formation yields (G (H_2O_2)) (nanomol/J) observed during the sonolysis of H_2O and H_2SO_4 under Ar/(20%)O_2 atmosphere at 20 °C as a function of the applied acoustic frequency.

*

f (kHz)	H_2O		0.5 mM H_2SO_4	
	Pure	With UO_2 (200mg)	Pure	With UO_2 (200mg)
20	0.1 ± 0.05	-	0.2 ± 0.1	-
100	1.3 ± 0.1	-	-	-
346	2.6 ± 0.3	1.6 ± 0.3	2.9 ± 0.3	1.9 ± 0.3
1047	1.9 ± 0.2	1.2 ± 0.1	2.2 ± 0.2	0.6 ± 0.1

Formation yields were calculated using the following formulae $\frac{W_o\ (H_2O_2)}{P_{ac} \times 60}$ where P_{ac} is the acoustic pressure.

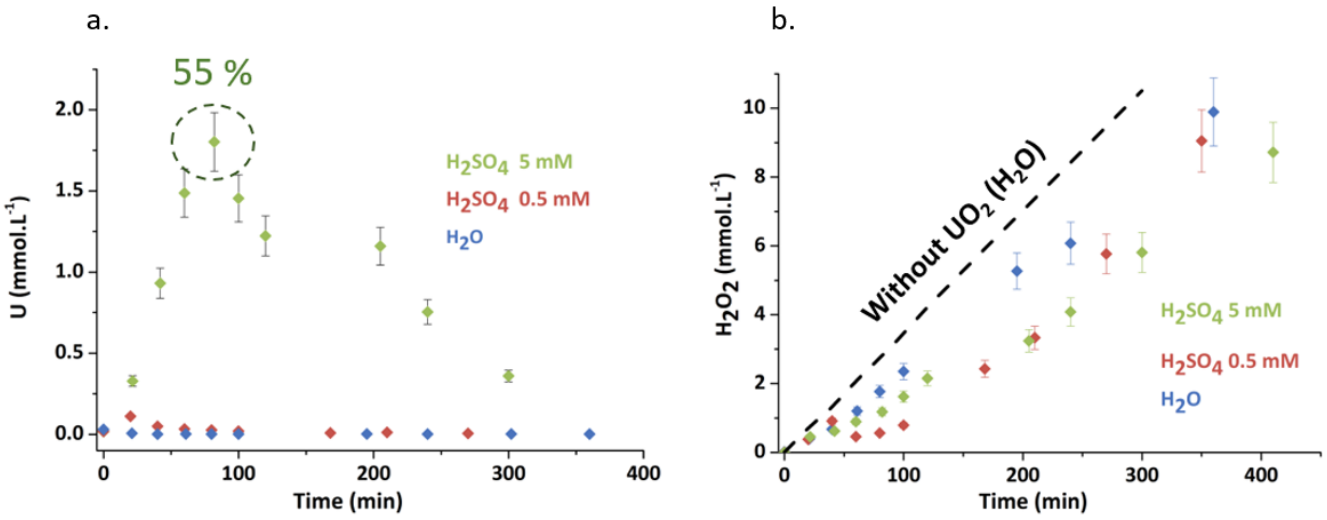

Figure 1: (a.) Concentration of uranium accumulated in solution as a function of time during the sonication of 200 mg UO_2 (fired at 800°C, 3 mM) in H_2O, 5 mM H_2SO_4 and 0.5 mM H_2SO_4 (346 kHz, 0.2 W.mL^{-1}, 20°C, Ar/(20%)O_2). (b.) Evolution of H_2O_2 concentration in solution for similar conditions.

PXRD analyses of the solid residues recovered after sonication are illustrated in **Fig. 2.a** and confirmed the *in-situ* formation of meta-studtite [$(UO_2)O_2(H_2O)_2$] in agreement with the literature (ICSD 01-081-9033).[11] Data processing allowed us to estimate the percentage of conversion of UO_2 into uranyl peroxide which varied as a function of the aqueous medium and treatment duration. In the experimental domain studied (6 h sonication), a complete conversion was observed for the most acidic conditions (pH = 2.2) which was explained by a better dissolution of UO_2 (**Fig. 1.a**) followed by the precipitation of accumulated uranyl ions into (meta-)studtite[27]. In these conditions, the behaviour of UO_2 agrees with the literature and the reactions **Eq. 12** and **Eq. 13**.[51] For softer acidic conditions, the conversion of UO_2 was not complete after 6 h sonication and reached ca. 88 and 77 wt.% of meta-studtite for 0.5 mM H_2SO_4 and H_2O, respectively. The absence of significant accumulation of uranium in solution for these conditions (**Fig. 1.a,b**) combined to the significant conversion of UO_2 to uranyl peroxide suggest a different behaviour directly related to the studtite solubility, the pH and H_2O_2 concentration. This behaviour is similar to that observed during the alteration of irradiated fuels under gamma irradiation.[52] An acidic pH combined with the formation of hydrogen peroxide by water radiolysis leads to an increase in the solubility of uranium

according to the solubility product K_{sp} of Eq. 10 ($K_{sp} = [UO_2^{2+}]\,[H_2O_2]/[H^+]^2$). The precipitation of uranium peroxide then occurs for high uranium concentrations and for significant oversaturations in solution. The concentrations in solution pass through a maximum above the solubility limit of uranyl peroxide and then decrease rapidly when the rate of condensation and growth of the nuclei increase. Conversely at a higher pH (5.8) the solubility of uranium is much lower, and the precipitation of uranyl peroxide occurs at low concentrations.

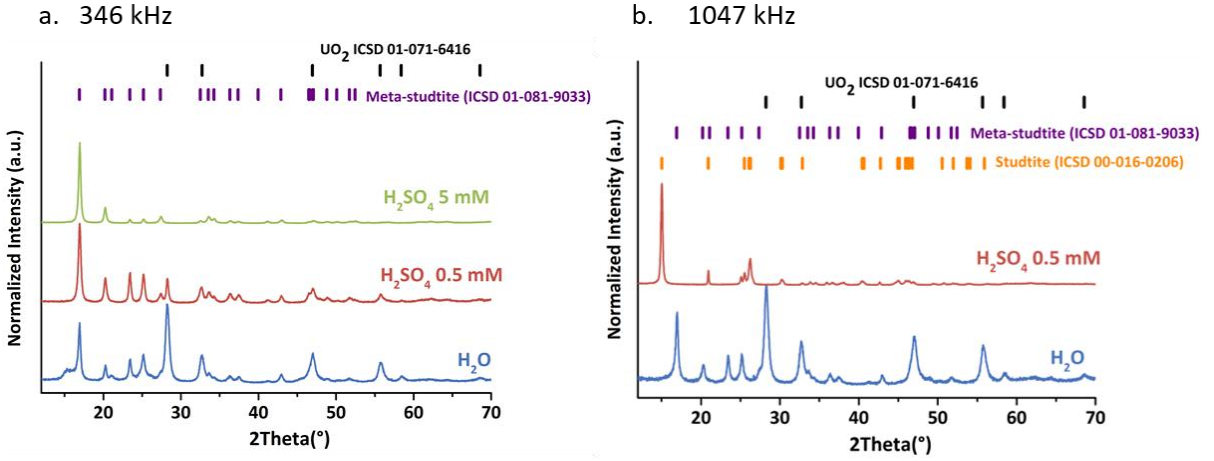

Figure 2: XRD diffractograms acquired on the solid phases after sonication of UO_2 (fired at 800°C, 3 mM) during 6 h at (a.) 346 kHz (0.2 W.mL^{-1}, 20°C, Ar/(20%)O_2) and (b.) 1046 kHz (0.16 W.mL^{-1}, 20°C, Ar/(20%)O_2).

Table 2 gathers thermodynamic data calculated for 346 kHz experiments. In pure water, the uranyl concentration in solution was found to be low (10^{-6} M) whatever the sonication duration. The associated strongly positive value of the studtite saturation index (SI>2) from the beginning of the experiment agree with a quick and local re-precipitation of studtite due to the poor solubility of UO_2 and studtite in these conditions. The very low concentration of calculated uranium aqueous species (< 10^{-6} M) is in agreement with the absence of uranium accumulating in solution for our experimental conditions. On the other hand, for 5 mM H_2SO_4 (pH = 2.2), the uranium rises to 10^{-4} M. In comparison to the experiment carried out in pure water, the saturation index value is lower (around SI= 1) and particularly low during the first 40 min of sonication). Under these conditions, uranium solubility is therefore higher (>10^{-4} M) as observed in the experiment. Nevertheless, this rise in concentration for aqueous uranium from low to higher acidic conditions may also be explained by the presence of small colloids of hydrated uranium including peroxides that would increase the apparent solubility of aqueous uranium.**[53] Fig. 3** gathers solubility diagrams in the three studied media using 346 kHz experiment data with the same H_2O_2 concentration (2 10^{-3} M). Pure water conditions favor studtite formation whereas sulfuric conditions describe a system at the solubility limit with the presence of $UO_2SO_{4(aq)}$ in solution (**Fig. 3.a** *vs.* **Fig 3.c**). Finally, **Fig. 3.b** depicts an intermediate system between the two previous ones.

Table 2: Concentration of uranium species released in solution as a function of H_2O_2 concentrations determined in solution during 346 kHz sonolysis in H_2O and H_2SO_4 under Ar/(20%)O_2 atmosphere at 20°C. Thermodynamic calculations for uranium were performed with CHESS, at the thermodynamic equilibrium and saturation indexes (SI) for Studtite (with K_s= 1.34 x 10^{-3} at 25°C)[54]

Time (min)	$[U_{tot}]_{exp}$ (M)	$[H_2O_2]_{exp}$ (M)	pH	$[UO_2^{2+}]_{(eq)}$ (M)	$UO_2(SO_4)_2^{2-}{}_{(eq)}$ (M)	$UO_2SO_{4(aq)}$ (M)	SI (Studtite) *Log Q/K_s*
	H_2O						
0	2 x 10^{-5}	0	5.8	1.68 x 10^{-7}	-	-	none*
300	2 x 10^{-6}	9 x 10^{-3}	3.7	5.97 x 10^{-9}	-	-	2.51
	5 10^{-4} M H_2SO_4						
0	2 x 10^{-5}	0	3.2	1.41 x 10^{-5}	2.24 x 10^{-8}	5.74 x 10^{-6}	none
20	10^{-4}	4 x 10^{-4}	3.2	1.99 x 10^{-6}	3.23 x 10^{-9}	8.21 x 10^{-7}	1.67

5

40	5×10^{-5}	9×10^{-4}	3.2	7.08×10^{-7}	1.15×10^{-9}	2.92×10^{-7}	1.72
170	8×10^{-6}	2×10^{-3}	3.2	3.02×10^{-7}	4.93×10^{-10}	1.25×10^{-7}	1.27
270	5×10^{-6}	6×10^{-3}	3.1	1.60×10^{-7}	2.52×10^{-10}	6.47×10^{-8}	1.34
	$5\ 10^{-3}$ M H_2SO_4						
0	2×10^{-5}	0	2.2	7.13×10^{-6}	3.61×10^{-7}	1.24×10^{-5}	none
40	9×10^{-4}	6×10^{-4}	2.2	2.37×10^{-4}	1.02×10^{-5}	3.84×10^{-4}	0.41
80	2×10^{-3}	1×10^{-3}	2.2	4.66×10^{-4}	1.71×10^{-5}	6.9×10^{-4}	1.02
120	1×10^{-3}	2×10^{-3}	2.2	6.69×10^{-5}	3.24×10^{-6}	1.11×10^{-4}	0.99
240	7×10^{-4}	4×10^{-3}	2.2	2.35×10^{-5}	1.17×10^{-6}	4.10×10^{-5}	1.12
300	4×10^{-4}	6×10^{-3}	2.2	1.40×10^{-5}	7.09×10^{-7}	2.45×10^{-5}	1.04

* Presence of schoepite

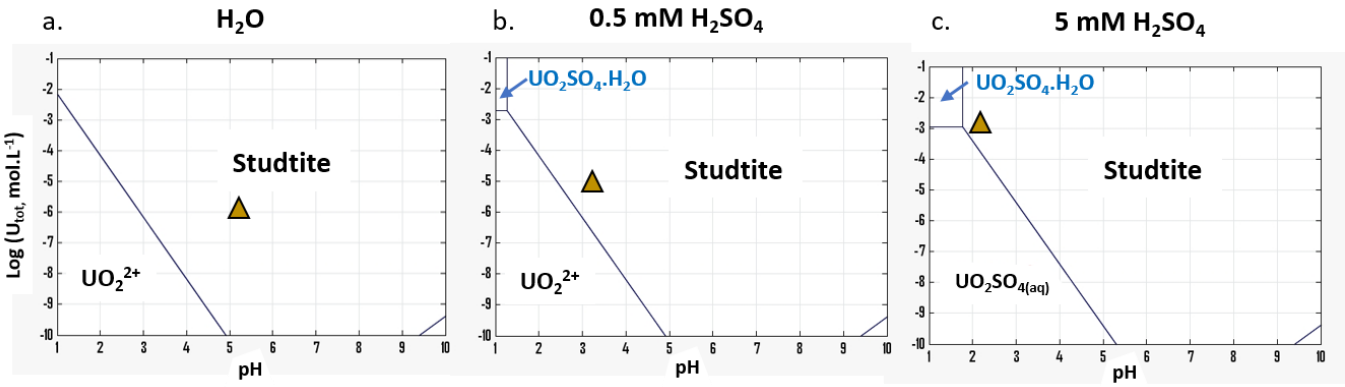

Figure 3: Solubility diagrams calculated for UO_2 as a function of pH at 25°C using CHESS software and data measured during 346 kHz sonolysis of UO_2 (0.2 W.mL^{-1}, 20°C, Ar/(20%)O_2) with H_2O_2 values: 2.10^{-3} M in (a.) H_2O, (b.) 0.5 mM H_2SO_4 and (c.) 5 mM H_2SO_4

$$UO_2^{2+} + 2\ SO_4^{2-} \longrightarrow UO_2(SO_4)_2^{2-} \qquad \text{Eq. 11}$$

To evaluate the influence of the ultrasonic frequency, the sonication of UO_2 powder was performed under similar conditions at 1047 kHz (20 °C, 6 h). **Fig. 4.a** displays the related accumulation kinetics for uranium in H_2O and 0.5 mM H_2SO_4. In these conditions, the accumulation rates and the maximum amount of uranium observed in solution were more important in acidic media and almost non-existent in pure water. The consumption of H_2O_2 was significant in both cases notwithstanding a lower rate in H_2O (**Fig. 4.b**) agreeing with the results observed at 346 kHz (**Fig. 1.b**). In agreement with the previous experiments, these observations were also accompanied by the modification of the color of the suspension and conversion of UO_2 into uranyl peroxide which was confirmed by PXRD **(Fig. 2.b)**, IR **(Fig. S4.a)** and Raman **(Fig. S4.b)**)[55]. Curiously, we obtained studtite at 0.5 mM H_2SO_4 and meta-studtite in H_2O for 1047 kHz experiment. This difference may be explained by subtle distinction in the experimental drying conditions.[56]

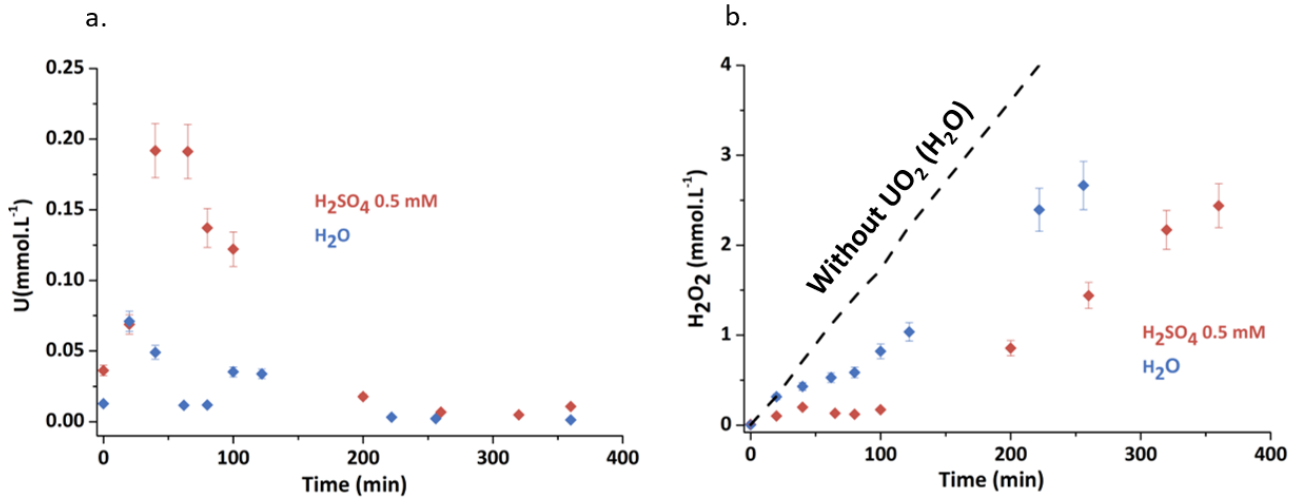

Figure 4: (a.) Concentration of uranium accumulated in solution as a function of time during the dissolution of 200 mg UO_2 (3 mM) in H_2O or 0.5 mM H_2SO_4 (1047 kHz, 0.15 W.mL^{-1}, 20°C, Ar/(20%)O_2). (b.) Evolution of H_2O_2 concentration in the similar media.

For both acoustic frequencies, the extremely low presence of U in pure water combined to the consumption of H_2O_2 and conversion into studtite suggest a different behavior between low and more acidic conditions. While concentrated H_2SO_4 conditions (5 mM) clearly involve the dissolution followed by reprecipitation of the neoformed phase, pure water conditions rather suggest a quick conversion occurring on surface and most likely attributed to a low dissolution rate of the oxide. **Fig. 4.b** shows two kinetic domains for H_2O_2 accumulation including an inhibition period in the 0-120 min range, followed by an almost linear accumulation rate after *ca.* 120 min (both rates remain lower than the one observed in the absence of UO_2 powder). Such a behaviour could be related to the conversion mechanism according to Clarens and al. studies suggesting that H_2O_2 oxidizes faster U(IV) than it dissolves UO_2.[48] The surface oxidation and conversion to a peroxide neophase being in competition with the dissolution reaction. The low dissolution rate expected for uranium oxide in such low acidic conditions in comparison to the precipitation kinetics of U(VI) peroxides may also contribute to this behaviour. Further experiments were also performed at 550 kHz leading to similar conclusions about U and H_2O_2 accumulation in solution, with a partial or total conversion of UO_2 into uranyl peroxide (**Fig. S5**).

3.2. Unusual morphology of uranyl peroxides formed under ultrasound

SEM investigations carried out on the recovered solids after sonication (346 kHz) evidenced different morphologies depending on the acidity of the system (**Fig. 5**). The solid sample obtained under the most acidic conditions (5 mM H_2SO_4, pH= 2.2) showed needle-like particles measuring ca. 5 µm long and agreeing with a dissolution/reprecipitation mechanism mentioned above **(Fig. 5.c)**. These needle-like morphologies are typical of the formation of uranyl peroxide observed during the oxidative dissolution of UO_2 in the presence of H_2O_2 both on single crystals[57] and on sintered pellets.[53] Such a morphology agrees with the monoclinic (C2/c) and orthorhombic natural structure of studtite or (meta-)studtite, respectfully, composed of uranyl polyhedral chains forming elongated crystals.[11,12] Interestingly, when the pH of the sonication experiment increased (0.5 mM H_2SO_4 at pH= 3.2 and H_2O at pH= 5.8), the neo-formed phase is found to be composed of squared platelet similar to the one of the initial UO_2 (**Fig. 5.a** *vs*. **5.c**). In agreement with PXRD measurements, these results demonstrate that the sonication of UO_2 at selected conditions allows a pseudomorphic transformation of UO_2 into (meta-)studtite. Surprisingly, the as-formed particles may be further drilled with a sub-micrometric hole in their exact centers (**Fig. 5.c**). It is worth noting that control experiments carried out with continuous addition of H_2O_2 reactant in the absence of ultrasound never led to such morphologies (**Fig. 5.b)**. Sonochemical conditions generated at UO_2 interface appear different from the chemistry induced by H_2O_2 addition at silent conditions. A similar conclusion comes out from radiolysis experiments which are also different with sonochemistry pointed in this work.[53]

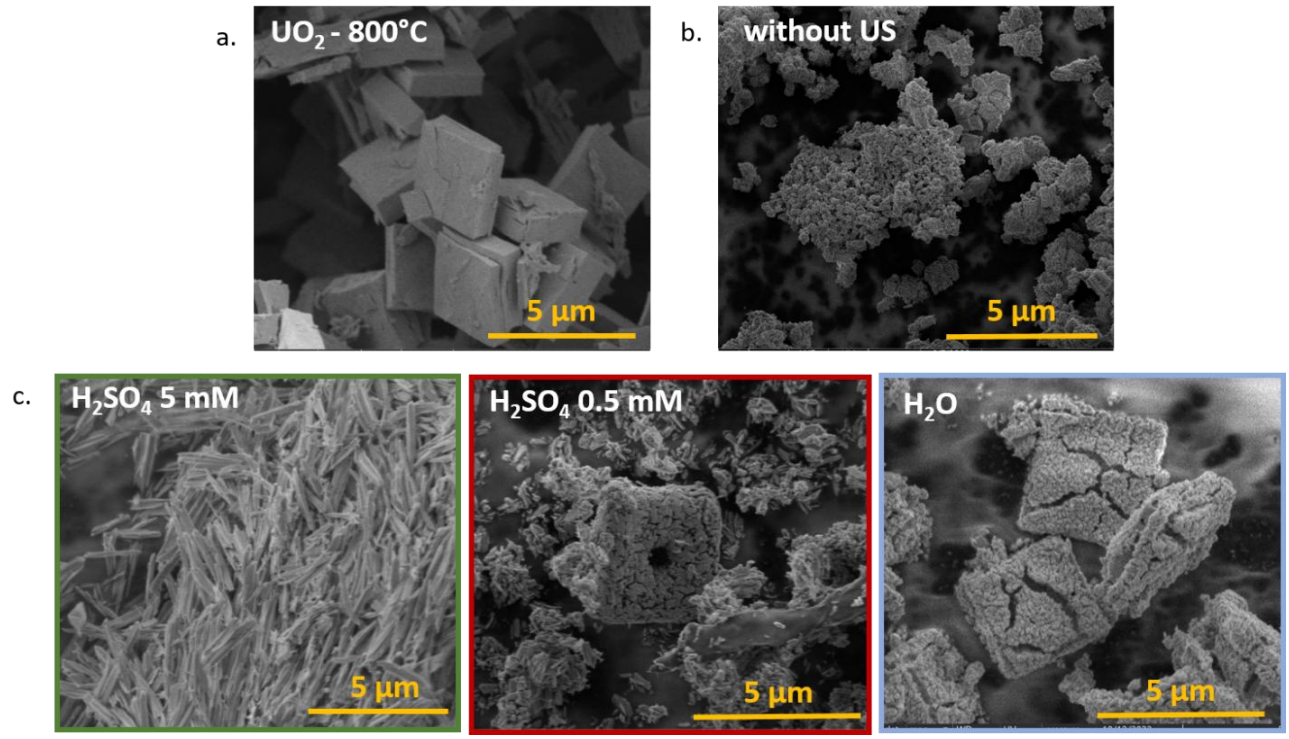

Figure 5: SEM images acquired on (a.) UO_2 reference synthetized by the oxalate route (800 °C, Ar/(4%)H_2), (b.) UO_2 after addition of H_2O_2 (12 mM, stirring) and (c.) the solid residues observed (0.2 W.mL^{-1}, 20°C, Ar/(20%)O_2) after 346 kHz sonication of UO_2 (3 mM, 200 mg, fired at 800°C) in H_2SO_4 (5 mM and 0.5 mM) and H_2O.

Similar experiments were carried out with an uranium oxide sample exhibiting a lower refractory behaviour towards dissolution. The latter was prepared under similar conditions with a lower firing temperature (485 °C). **Fig 6** presents SEM images corresponding to the sonolysis residue treated in pure water at 346 kHz and 1047 kHz with similar other conditions. In both cases, a similar behavior was observed for uranium and H_2O_2 with the observation of a partially converted studtite (80 wt.%) including a similar perforated platelet morphology. These holes were not found in the experiment carried out with UO_2 fired at 800 °C and sonicated at 346 kHz (**Fig 5.c**). Such a behavior suggests that refractoriness of the starting oxides impacts pseudomorphic transformation rate and progress. A summary of the main experiments carried out in this study is provided in the **Table 3**.

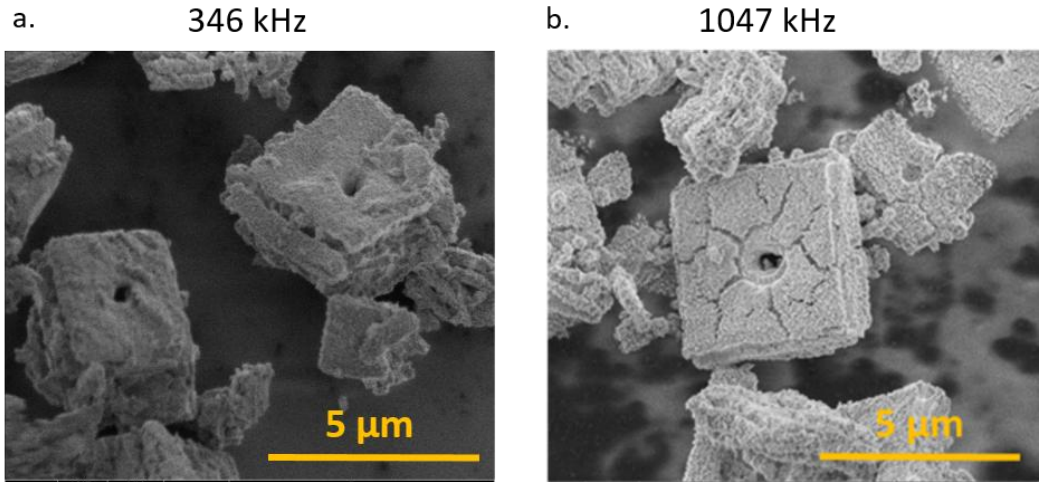

Figure 6. SEM images of the solid residue recovered after sonication of UO_2 fired at 485 °C in pure water (3 mM, 200 mg, 20 °C, Ar/(20%)O_2) at (a.) 346 kHz (0.2 W.mL^{-1}) and (b.) 1047 kHz (0.15 W.mL^{-1})

Table 3: Summary of the experiments as a function of the used oxide, ultrasonic frequency and medium (20°C, Ar/(20%)O_2)

Oxide Refractoriness to dissolution	Frequency (kHz)	Media	Conversion rate after 6 h	Morphology	Center Hole
UO_2 - 485 °C	0	0.5 mM H_2SO_4	Na	Random	-
	346	H_2O	Na	Pseudomorph	X
		0.5 mM H_2SO_4	> 98 % (12h)	DR + ε Pseudomorph	X
	505	0.5 mM H_2SO_4	Na	Pseudomorph + DR	X
	1047	H_2O	Na	Pseudomorph	X
UO_2 - 800 °C	0	H_2O	Na	Random	-
		0.5 mM H_2SO_4	> 98 %	Random	-
	20	0.5 mM H_2SO_4	35 %	Pseudomorph + DR	-
	346	H_2O	77%	Pseudomorph	-
		0.5 mM H_2SO_4	88 %	Pseudomorph + DR	X
		5 mM H_2SO_4	100 %	Needles	X
	1047	H_2O	45 %	Pseudomorph	X
		0.5 mM H_2SO_4	Na	DR + ε Pseudomorph	X

DR: desert rose

Further AFM analyses performed on the UO_2 squared platelets fired at 485 °C (**Fig 7.a)** and the holed peroxide pseudomorphs demonstrated that the latter was covered with small needle-like particles **(Fig 7.c**). It was demonstrated that the presence of these needle-like crystals increased the local surface roughness when compared to initial UO_2 (R_a= from 4 to 43 nm and R_q= from 5 to 51 nm) **(Fig 7.b** *vs.* **d).** 3D reconstructions from SEM images of studtite obtained after sonolysis at 550 kHz of UO_2 for 7 h are shown in **Fig 7.e** illustrating a complete hole in the center of the plate and the high roughness caused by the formed peroxide crystals.

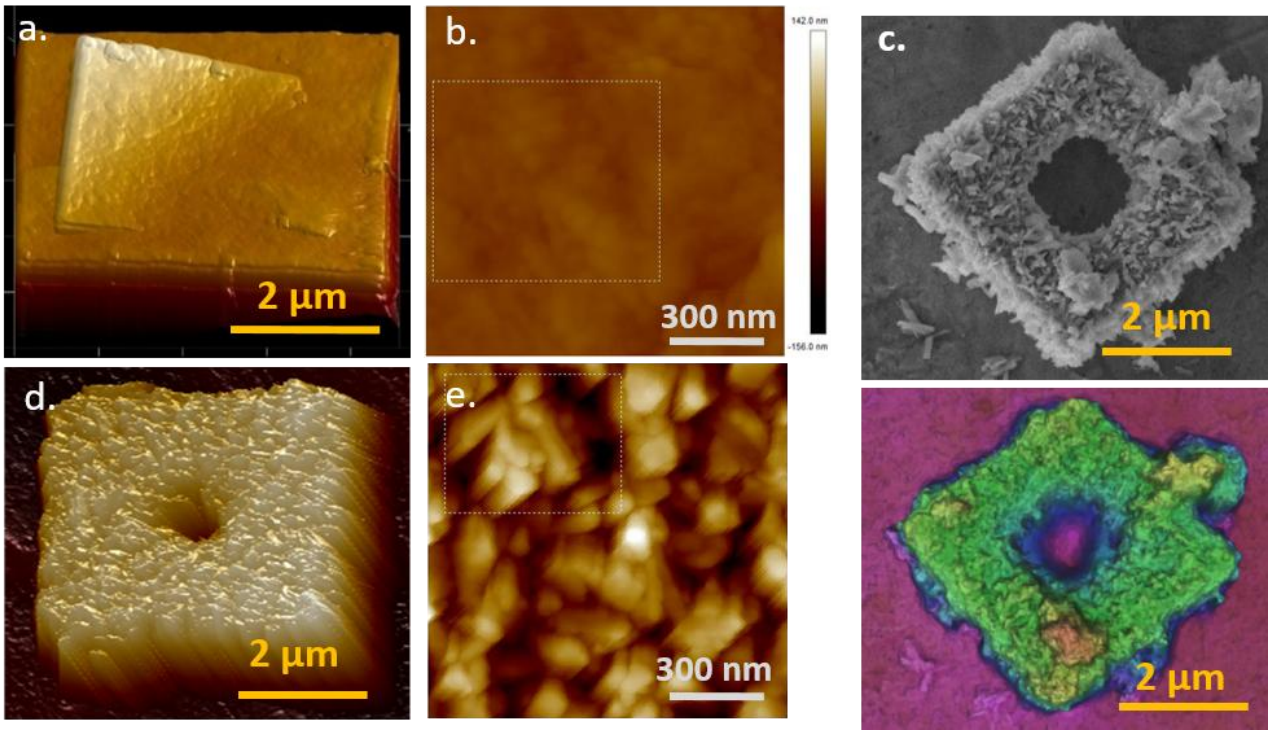

Figure 7: AFM images acquired on (a., b.) initial UO_2 and (c., d.) the corresponding solid residues (studtite) recovered after 505 kHz sonication in 0.5 mM H_2SO_4 (200 mg, 3 mM, 20°C, Ar/(20%)O_2, 7 h). (e.) SEM image and 3D reconstruction of a holed studtite pseudomorph.

To better evaluate the effect of the acoustic frequency, further experiments were carried out in the 20 - 1047 kHz range under similar conditions (3 mM UO_2, 20°C, Ar/(20%)O_2, 0.5 mM H_2SO_4, **Fig. 8**). The holed platelets were only observed after sonication at 346, 505 and 1047 kHz (*i.e.,* at high frequencies) contrasting with the experiments performed in the absence of ultrasound or at 20 kHz and 100 kHz (*i.e.,* at low frequencies). Such a behaviour indicates that the formation of the hole is related to the acoustic cavitation phenomenon which only appears significant for high frequency ultrasound (≥ 346 kHz). Usually, low frequency ultrasound provides stronger physical effects (e.g., dispersion, erosion and fragmentation of particles) which are less important at high frequency ultrasound where chemical effects (including the formation of H_2O_2) can be dramatically enhanced. AFM, SEM and 3D reconstructions allowed further characterizations for this unprecedented morphology and confirmed that the central hole passes through the entire platelet (**Fig. 7)**. Noteworthy, complementary experiments **(Fig. S6)** performed in dilute nitric acid showed very different shapes with a very bad conversion rate into metastudtite, possibly attributed to parasite NO_x reactions arising from sonolytic decomposition of NO_3^- and HNO_3.[29,48,49]

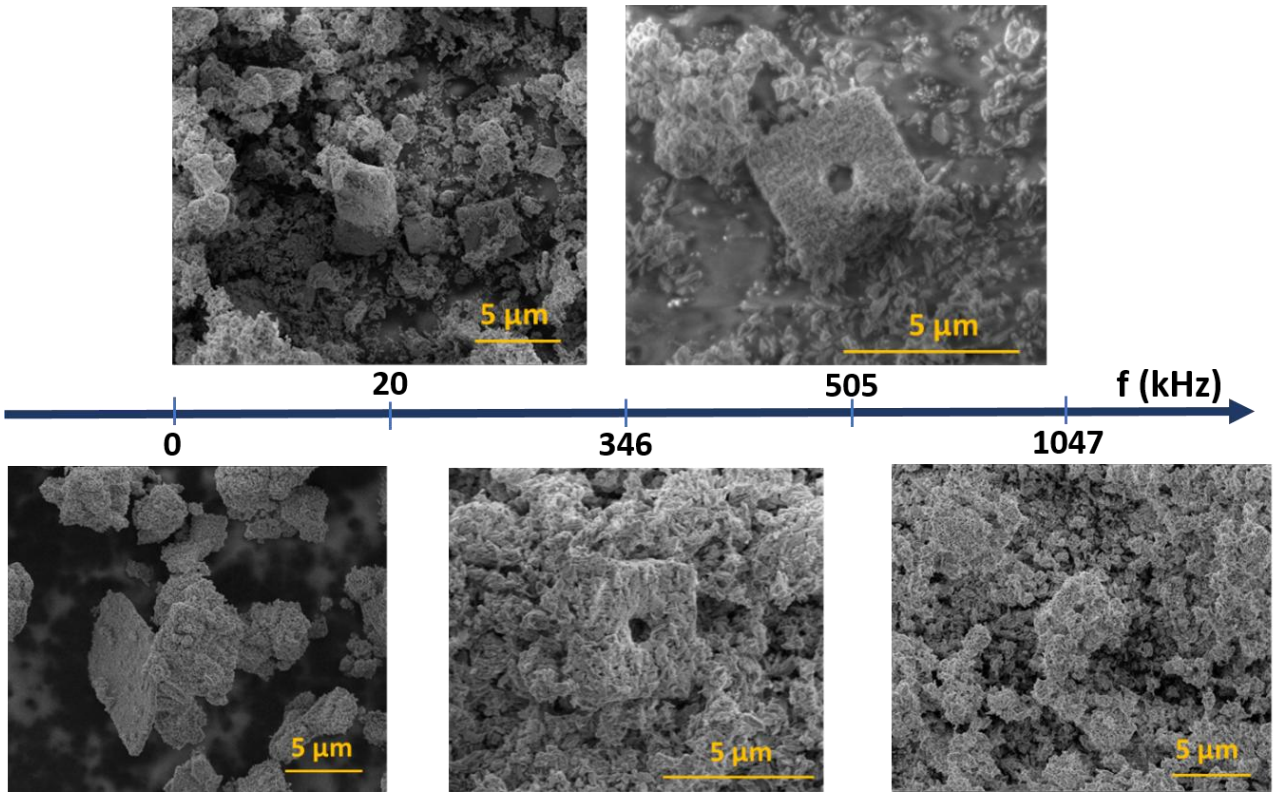

Figure 8: SEM images acquired on the solid residues for UO_2 fired at 800 °C in 0.5 mM H_2SO_4 (200 mg, 3 mM, 20°C, Ar/(20%)O_2) after treatment at 20, 346, 505, 1047 kHz and in the absence of ultrasound.

Fig. 9 illustrates the time-dependent transformation of UO_2 surface morphology observed during its high-frequency sonication in 0.5 mM H_2SO_4. The typical smooth and flat squared platelet of initial UO_2 can be observed for the initial sample. An oxidation layer attributed to (meta-)studtite rapidly forms on the surface of the samples after 1 h sonication and traces of alteration (orange arrows) can be observed in the center of some platelets. After 95 min, this alteration becomes more important and propagates through the first layers of the platelet in their center and a hole begins to form. Generally, the rest of the surface is poorly modified anymore, and we can notice the progressive drilling of the surface center, leading to a completely holed surface after 360 min sonication.

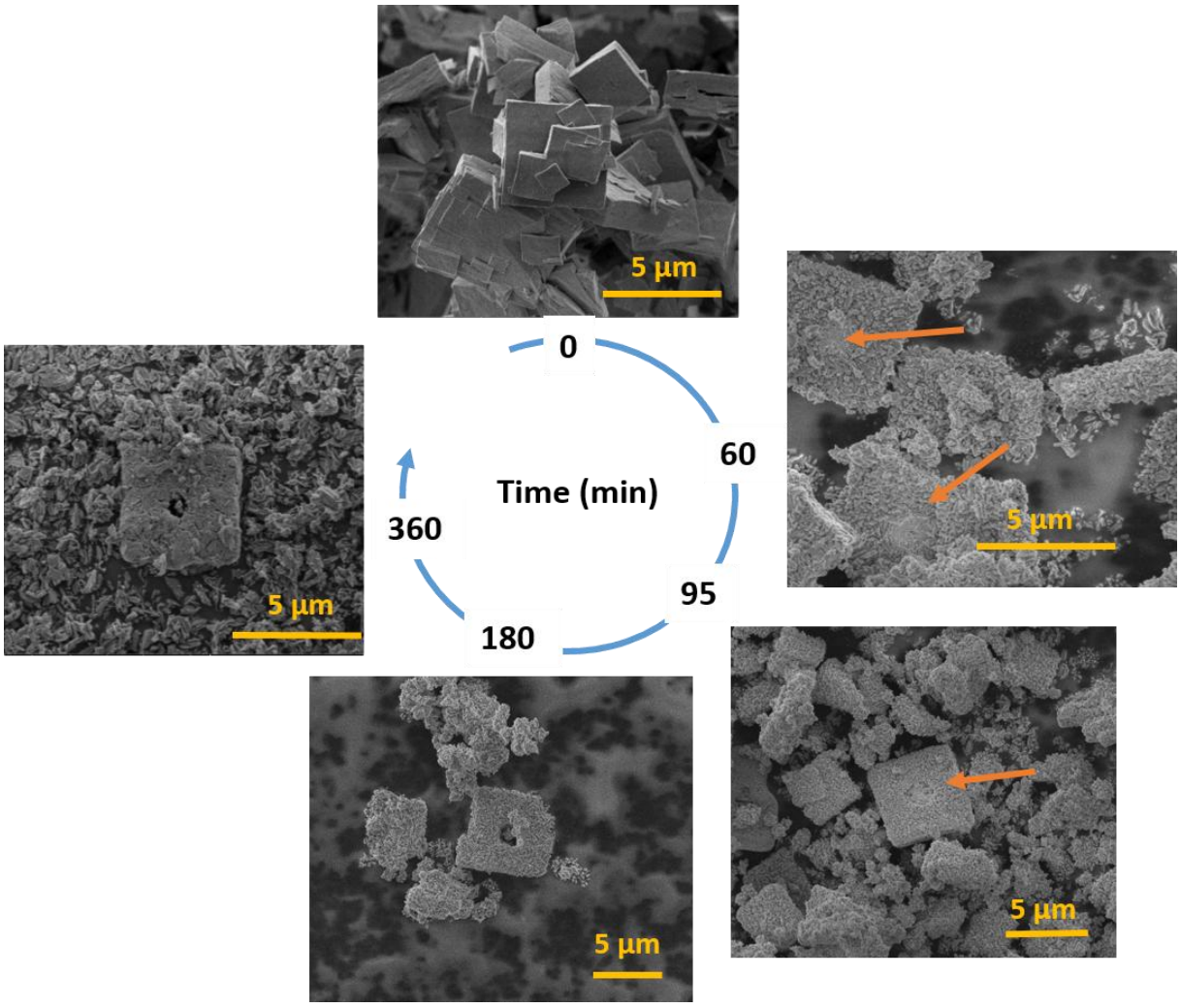

Figure 9: SEM image of the solid residue evolution observed after 346 kHz sonication of UO_2 (200 mg, 3 mM) in 0.5 mM H_2SO_4 (0.2 W.mL^{-1}, 250 mL, 20°C, Ar/O_2).

3.3. Suggested conversion mechanism and pseudomorph origins

Several consecutive reactions are controlling the conversion of the oxide into uranyl peroxide: (i) the oxidation of U(IV) into U(VI), (ii) the dissolution of uranium species associated with its transfer in the solution as an uranyl ion **(Eq 4-7)** and (iii) its precipitation into uranyl peroxide **(Eq 13)**. These reactions are regulated by the available concentration of H_2O_2 and the acidity of the medium. Consumption of hydrogen peroxide was noticed for all the experiments with a higher rate in the most acidic conditions compared to water. Such an observation confirms a significant effect of the pH in the above discussed reactions. For an acidic environment, where the saturation index of the solution (SI) is the lowest, the dissolution is therefore more efficient so as the accumulation of uranium in solution (**Fig. 1**). As the dissolution kinetics are faster, the destruction of the starting oxide is more important leading to a complete dissolution followed by re-precipitation in agreement with the observation of dispersed needle-like particles. By contrast, in a less acidic environment (H_2SO_4 0.5 mM and H_2O) the slower dissolution releases lower amounts of U in solution which immediately precipitate due to an excess of peroxides in the surroundings, which is in agreement with the evidenced absence of U in solution. Such a behavior would explain a surface re-precipitation phenomenon agreeing with SEM observations (after 1 h sonolysis) in

water and 0.5 mM H_2SO_4 (**Fig. S7**). Thermodynamic calculations also confirmed the decrease of uranium peroxide solubility with the rising pH.[48] Note also, some mechanisms have been proposed in the literature about the formation of peroxidic species on surface from oxo precursor or dissolution mechanism in acidic media.[26]

The formation of the peroxide pseudomorphs can be explained by a sono-capillary effect which would enable the circulation of the reactants in the volume of the initial UO_2 platelets. Such a mechanism is made possible by the foliated morphology of the oxides confirmed by SEM and TEM images (**Fig. 10.a, c**). Such morphology results from the firing conditions of the foliated U(IV) oxalate precursors going with the formation of very small coherent domains in the final oxide. Sono-capillary effect, which consist in an inrush of liquid at a capillary entrance resulting from bubble collapses driven by the action of ultrasound, may contribute to the circulation of the reactants (*e.g.* U, H_2O_2, H^+) into small interstices acting as capillary channels. Tzanakis et al. described a similar phenomenon using a liquid metal melt to fill the preexisting grooves of an Al-Cu melt.[60] Results allowed to attribute this phenomenon to the implosion of cavitation bubbles at the opening of the grooves also acting as capillaries. Nikolai and Valeri reported the ultrasound-enhanced penetration of fluorescent liquid dyes into micro-cracks cavities that they attributed to ultrasonic capillary effect independently on the surface tension of the liquid and wettability of the cracks.[61] In our conditions, this effect can be strengthened by density differences between UO_2 (9.99 $g.cm^{-3}$) and U(VI) peroxides (3.7 $g.cm^{-3}$) that would also favor the formation of porosities in foliated UO_2.[62–64]

The resulting swelling of the platelet particles is clearly observed in **Fig. 6** for UO_2 sonicated in pure water. Additional TEM images performed on a thin section (lamella) of a platelet sonicated in water (prepared using FIB-SEM) revealed the presence of contrasted sheets or layers differing with the homogeneous oxide observed before treatment. Such an observation confirms the volume conversion of UO_2 and suggest that it occurs by the pushing of reactants between the UO_2 sheets that convert into lower density peroxides (**Fig. 10.d** and **Fig 11**). In acidic environment, protons allow an easier leaching of the uranyl ions located in the foliated material as evidenced in **Fig. 5**. Sono-capillary effect would help in the circulation of the reactants and explain the observed pseudomorphic conversion of UO_2 into U(IV) peroxides. A complementary study (not presented here) also demonstrated that sulfate concentration is not significant towards the morphology conservation in agreement with the literature.[27] Note that for most of our experiments, UO_2 conversion yielded meta-studtite rather than studtite. The predilection of one phase against the other is not yet very clear and most probably results from drying conditions.[65]

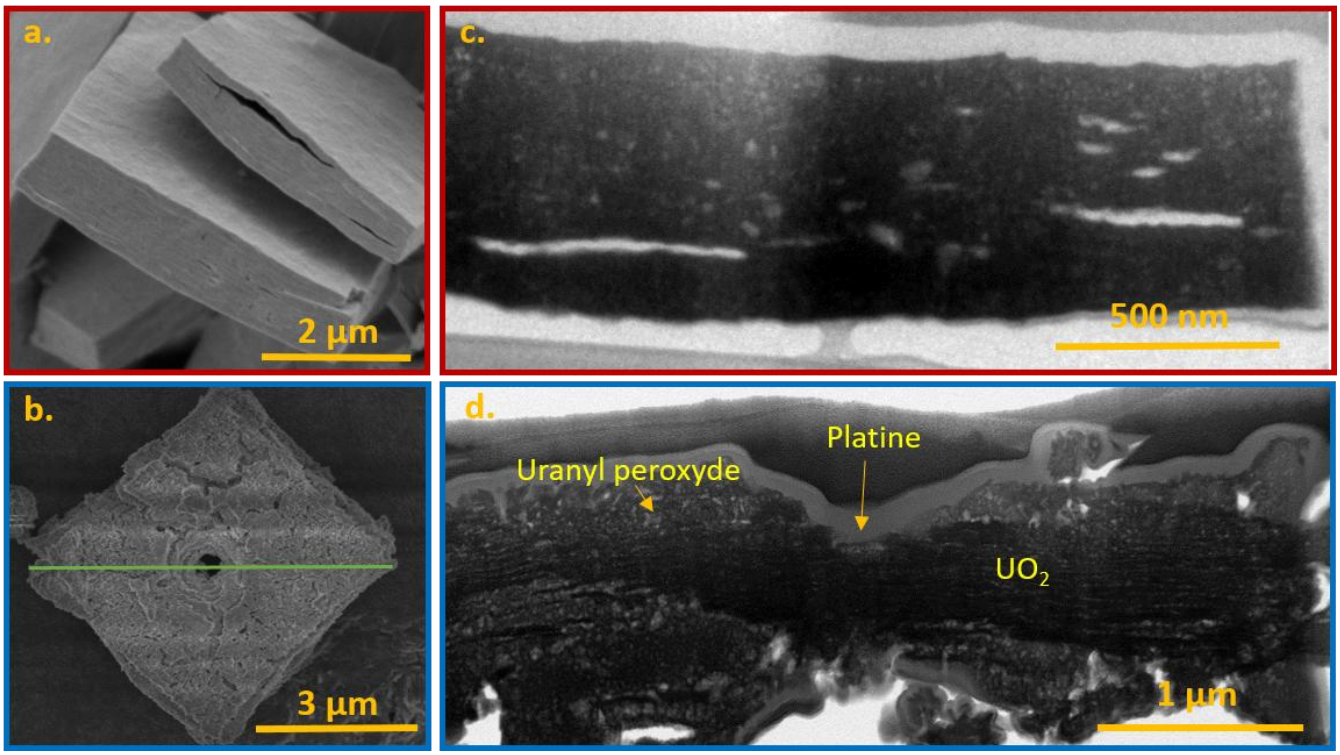

Figure 10: SEM images acquired on (a.) UO_2 reference synthetized by the oxalate route (485°C, Ar/(4%)H_2) and (b.) a solid residue observed after 346 kHz sonication of UO_2 (0.2 $W.mL^{-1}$, 250 mL, 20°C, Ar/O_2) in pure water. (c.) and (d.) TEM images acquired on thin sections of respectively (a.) and (b.) prepared by FIB-SEM. The green line indicates approximately the location of the thin section.

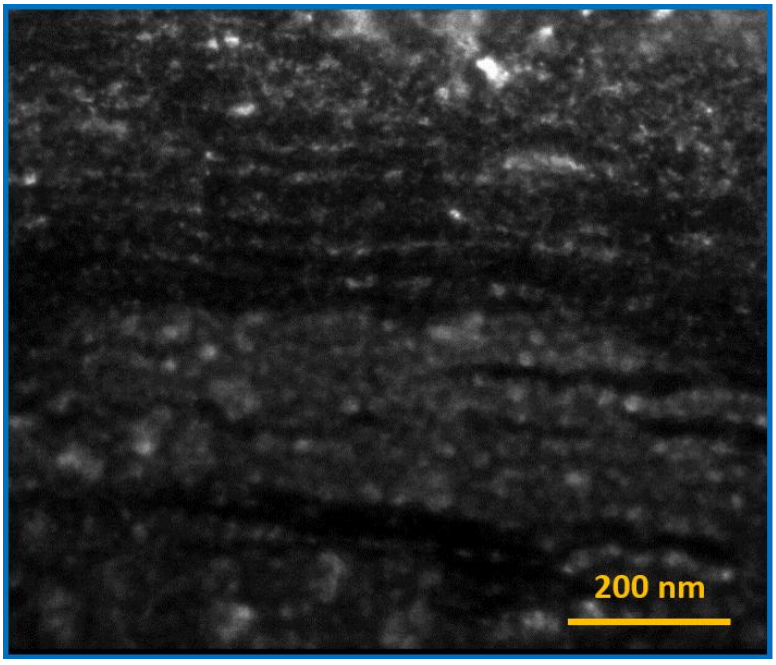

Figure 11: TEM observation of a thin section (FIB-SEM) of a sonicated UO_2 platelet in pure water (346 kHz, 0.2 $W.mL^{-1}$, 250 mL, 20°C, Ar/O_2).

3.4. Hole formation

Concerning the hole, we only note its appearance for ultrasonic frequencies higher than 346 kHz (not observed for 20 and 100 kHz experiments). Solids observed for low frequency experiments (SEM) are indeed only remnants of UO_2 that has not been fully converted **(Fig. S6)** and are far less homogeneous than those obtained under high frequency ultrasound. Several parameters can influence this discrepancy: first, the important physical effects driven by low frequency ultrasound break up the platelets and avoid the morphological conservation.[36,40] Secondly, the deficiency in H_2O_2 formation for low frequency experiments does not allow a conversion as fast and complete as it is observed for high frequency experiments where H_2O_2 formation rate is higher. Third, the specific acoustic pressure and acoustic intensity **(Table 4)** estimated using **Eq. 14** with the plane waves assumption, may provide a good penetration of reactants in the solid volume (sono-capillary effect) while preserving the morphology of the sample when compared to 20 and 100 kHz experiments.

$$I = \frac{P^2}{2\rho c} \qquad \text{Eq. 14}$$

Where, I is the sound intensity (W.m^{-2}), P the sound pressure (Pa), ρ the density of water (1000 kg·m^{-3}) and c, the speed of sound in the medium (1480 m.s^{-1} in water).

Many hypotheses have been proposed to explain the formation of a hole in the center of the platelets including Kirkendall effect,[66] galvanic exchange,[66] mechanical traction,[67,68] etc. These hypotheses were not compelling regarding the sonication-dependent effects revealed in the studied system. The progressive formation of the holes noticed in **Fig. 9** strengthens their relation with the physical effects of ultrasound. The clarification of the mechanism is still in progress but some observations pave the way for a relevant explanation.

Table 4: Comparison of various parameters affected by the applied acoustic frequency.

f (kHz)	Acoustic intensity (W.m^{-2})	*Acoustic power P_{ac} (W.mL^{-1})	Acoustic pressure P (P_a)	**Bubble resonant size R_{max} (µm)
20	1.7 x 10^5	0.35 ± 0.05	7.2 x 10^5	150
100	3.4 x 10^3	0.12 ± 0.05	1.0 x 10^5	20
346	1.9 x 10^4	0.20 ± 0.05	2.4 x 10^5	8
1047	1.5 x 10^4	0.15 ± 0.05	2.1 x 10^5	3

* computed with calorimetric method;[43] **estimated using Minnaert's equation in agreement with literature[69]

One hypothesis could be related to repeated impacts associated with the asymmetric implosion of cavitation bubbles, referred to as liquid micro-jets.[32,36,70] Usually, this effect is associated with low frequency ultrasound but examples of cavities produced by micro-jets in materials at high frequency have been put forward by recent studies.[71–73] In particular, Sugino and Yamamoto reported the effects of ultrasound ranging from 26 kHz to 3.6 MHz on starch material and proposed several important parameters to explain the pit formations

including the size ratio between the cavitation bubble and the surface, the object's physical characteristics and the distance of the bubble from its surface.[72] In our case, as the uranium layers are oxidized and become more vulnerable (see density above), they are more likely to break under the mechanical pressure generated by these oriented jets which can go up to 100 m/s and a wild range of depths and diameter holes.[70,71] Therefore, low frequency ultrasound (20 and 100 kHz) provides bubbles that are too large (and violent) compared to the size of the oxides (*ca.* 4-6 µm). Furthermore, holes are only observed for 4-6 µm particles, even if there is a slight disparity in the size of the platelets in the starting oxide (**Fig S2.b**). This indicates that only one specific size range of platelets with respect to the bubbles can undergo this phenomenon, supporting our hypothesis. The main question concerning this possibility is the location of the hole, which is always in the centre of the substrate. Recent papers dedicated to the fundamental understanding of micro-jet demonstrated that edge effects play a significant role on the orientation of the micro-jet, as well as the implosion symmetry of the bubble as a function of the object/bubble size ratio, the distance between them and the geometry of the surface.[74,75] However, given the probabilities for this type of event to occur, it is very unlikely that holes are related to micro-jets.

Another hypothesis is rather related to gradients of reactant concentrations in the samples that would result from a progressive conversion of the oxide into peroxides. As seen previously, high frequency ultrasound (346 and 1047 kHz) may provide a good penetration of reactants in the solid volume with sono-capillary effect while preserving the solid integrity (**Table 3**).[32,64] Once peroxide forms, protons are generated in accordance with **Eq. 13** (step 1 on **Fig. 12)**. Sono-capillary effect driven by the local acoustic pressure could then push reactants (H^+, H_2O_2) in the solid volume (step 2). Introduced reagents can then react with UO_2 in the spaces according to **Eq. 12** producing uranyl ions which are further pushed towards the center of the platelet (step 3). Uranyl peroxide would then precipitate at UO_2 surface and participate in the opening of the grooves in the sample. In accordance with **Eq. 13**, the peroxide formation consumes H_2O_2 and releases protons that can be sonochemically-pushed towards the center thereby giving a gradient of reactant concentrations (step 4). In such conditions, the acidity of the platelet center would be stronger and very prone to dissolution also involving a higher solubility of peroxides as discussed in the first part of this study. Such conditions would favor a hole formation in the platelet center (step 5).

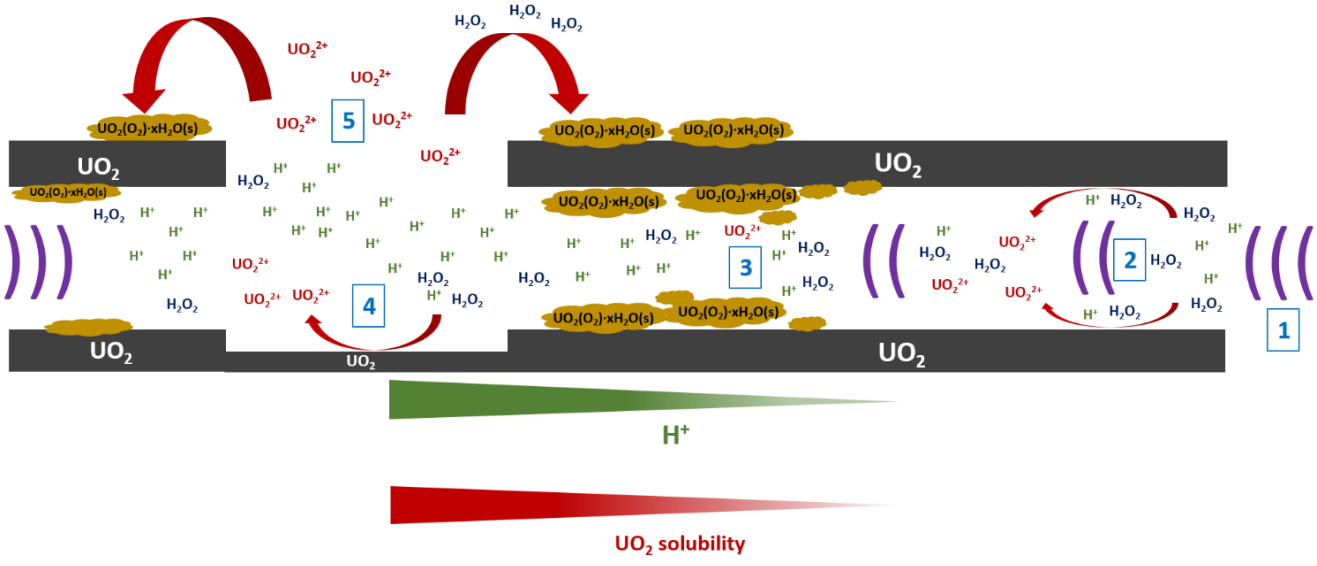

Figure 12: proposed scheme depicting the formation of the platelet center hole.

4. Conclusion

This work describes the sonochemical conversion of powdered UO_2 into uranyl peroxides ((meta-)studtite) in dilute aqueous media saturated with Ar/(20%)O_2 at 20 °C. While strongly acidic conditions resulted in the precipitation of needle-like peroxide particles, milder pH conditions yielded peroxide pseudomorphs which formation depends on the applied acoustic frequency and the *in-situ* generation of H_2O_2. Pseudomorphic transformation was demonstrated to be driven by the acoustic cavitation phenomenon and suggested to result more precisely from sono-capillary effect. The additional formation of a unique hole in the centre of the platelets was suggested to result from a gradient of reactant concentration most probably contributing in an increase of acidity and peroxide solubility in the centre of the samples. The clarification of the formation mechanism appears complex and the influence of the medium composition, the considered solids and the applied acoustic frequency will be investigated in details. Complementary experiments involving other particle shapes in the micrometric range appear particularly relevant. Up to our knowledge, ultrasound-assisted pseudomorphic conversion is an uncovered topic auguring exciting opportunities in the next future.

Acknowledgement

We acknowledge CEA RCHIM/RTA (cross-cutting basic research program). We would like to thank Joseph Lautru (ICSM Marcoule), Renaud Podor (ICSM Marcoule) and Michael Odorico (ICSM Marcoule) for their help in SEM and AFM characterizations. We also acknowledge Martiane Cabié (CP2M Aix-Marseille university) for FIB-SEM investigations.

References

[1] S. Nilsson, M. Jonsson, H_2O_2 and radiation induced dissolution of UO_2 and SIMFUEL pellets, J. Nucl. Mater. 410 (2011) 89–93. https://doi.org/10.1016/j.jnucmat.2011.01.020.

[2] S.T. Barlow, D.J. Bailey, A.J. Fisher, M.C. Stennett, C. Gausse, H. Ding, V.A. Krasnov, S.Y. Sayenko, N.C. Hyatt, C.L. Corkhill, Synthesis, characterisation and corrosion behaviour of simulant Chernobyl nuclear meltdown materials, Npj Mater. Degrad. 4 (2020) 3. https://doi.org/10.1038/s41529-020-0108-z.

[3] J. Qiu, P.C. Burns, Clusters of Actinides with Oxide, Peroxide, or Hydroxide Bridges, Chem. Rev. 113 (2013) 1097–1120. https://doi.org/10.1021/cr300159x.

[4] G. Sattonnay, C. Ardois, C. Corbel, J.F. Lucchini, F. Garrido, D. Gosset, Alpha-radiolysis effects on UO_2 alteration in water, J. Nucl. Mater. 228 (2001) 11–19.

[5] K. Maher, J.R. Bargar, G.E. Brown, Environmental Speciation of Actinides, Inorg. Chem. 52 (2013) 3510–3532. https://doi.org/10.1021/ic301686d.

[6] S.C. Smith, S.M. Peper, M. Douglas, K.L. Ziegelgruber, E.C. Finn, Dissolution of uranium oxides under alkaline oxidizing conditions, J. Radioanal. Nucl. Chem. 282 (2009) 617–621. https://doi.org/10.1007/s10967-009-0182-8.

[7] D.W. Shoesmith, Fuel corrosion processes under waste disposal conditions, J. Nucl. Mater. 282 (2000) 1–31. https://doi.org/10.1016/S0022-3115(00)00392-5.

[8] J.W.T. Spinks, R.J. Woods, An introduction to radiation chemistry, Third edition, 1990.

[9] E. Ekeroth, O. Roth, M. Jonsson, The relative impact of radiolysis products in radiation induced oxidative dissolution of UO2, J. Nucl. Mater. 355 (2006) 38–46. https://doi.org/10.1016/j.jnucmat.2006.04.001.

[10] K.-W. Kim, J.-T. Hyun, K.-Y. Lee, E.-H. Lee, K.-W. Lee, K.-C. Song, J.-K. Moon, Effects of the different conditions of uranyl and hydrogen peroxide solutions on the behavior of the uranium peroxide precipitation, J. Hazard. Mater. 193 (2011) 52–58. https://doi.org/10.1016/j.jhazmat.2011.07.032.

[11] P.C. Burns, K.-A. Hughes, Studtite, $[(UO_2)(O_2)(H_2O)_2](H_2O)_2$: The first structure of a peroxide mineral, Am. Mineral. 88 (2003) 1165–1168. https://doi.org/10.2138/am-2003-0725.

[12] P.F. Weck, E. Kim, C.F. Jové-Colón, D.C. Sassani, Structures of uranyl peroxide hydrates: a first-principles study of studtite and metastudtite, Dalton Trans. 41 (2012) 9748. https://doi.org/10.1039/c2dt31242e.

[13] F. Clarens, J. de Pablo, I. Díez-Pérez, I. Casas, J. Giménez, M. Rovira, Formation of Studtite during the Oxidative Dissolution of UO_2 by Hydrogen Peroxide: A SFM Study, Environ. Sci. Technol. 38 (2004) 6656–6661. https://doi.org/10.1021/es0492891.

[14] B.D. Hanson, B. McNamara, E.C. Buck, J.I. Friese, E. Jenson, K. Krupka, B.W. Arey, Corrosion of commercial spent nuclear fuel. 1. Formation of studtite and metastudtite, Radiochim. Acta. 93 (2005) 159–168. https://doi.org/10.1524/ract.93.3.159.61613.

[15] T. Vitova, I. Pidchenko, S. Biswas, G. Beridze, P.W. Dunne, D. Schild, Z. Wang, P.M. Kowalski, R.J. Baker, Dehydration of the Uranyl Peroxide Studtite, $[UO_2(\eta^2\text{-}O_2)(H_2O)_2]\cdot 2H_2O$, Affords a Drastic Change in the Electronic Structure: A Combined X-ray Spectroscopic and Theoretical Analysis, Inorg. Chem. 57 (2018) 1735–1743. https://doi.org/10.1021/acs.inorgchem.7b02326.

[16] T.L. Spano, J.L. Niedziela, A.E. Shields, J. McFarlane, A. Zirakparvar, Z. Brubaker, R.J. Kapsimalis, A. Miskowiec, Structural, Spectroscopic, and Kinetic Insight into the Heating Rate Dependence of Studtite and Metastudtite Dehydration, J. Phys. Chem. C. 124 (2020) 26699–26713. https://doi.org/10.1021/acs.jpcc.0c09082.

[17] C.R. Armstrong, M. Nyman, T. Shvareva, G.E. Sigmon, P.C. Burns, A. Navrotsky, Uranyl peroxide enhanced nuclear fuel corrosion in seawater, Proc. Natl. Acad. Sci. 109 (2012) 1874–1877. https://doi.org/10.1073/pnas.1119758109.

[18] A. Barreiro Fidalgo, Y. Kumagai, M. Jonsson, The role of surface-bound hydroxyl radicals in the reaction between H_2O_2 and UO_2, J. Coord. Chem. 71 (2018) 1799–1807. https://doi.org/10.1080/00958972.2018.1466287.

[19] Y. Kumagai, A. Barreiro Fidalgo, M. Jonsson, Impact of Stoichiometry on the Mechanism and Kinetics of Oxidative Dissolution of UO_2 Induced by H_2O_2 and γ-Irradiation, J. Phys. Chem. C. 123 (2019) 9919–9925. https://doi.org/10.1021/acs.jpcc.9b00862.

[20] S.M. Peper, L.F. Brodnax, S.E. Field, R.A. Zehnder, S.N. Valdez, W.H. Runde, Kinetic Study of the Oxidative Dissolution of UO_2 in Aqueous Carbonate Media, Ind. Eng. Chem. Res. 43 (2004) 8188–8193. https://doi.org/10.1021/ie049457y.

[21] M.E. Torrero, E. Baraj, J. de Pablo, J. Giménez, I. Casas, Kinetics of corrosion and dissolution of uranium dioxide as a function of pH, Int. J. Chem. Kinet. 29 (1997) 261–267. https://doi.org/10.1002/(SICI)1097-4601(1997)29:4<261::AID-KIN4>3.0.CO;2-S.

[22] A.C. Maier, E.H. Iglebaek, M. Jonsson, Confirming the Formation of Hydroxyl Radicals in the Catalytic Decomposition of H_2O_2 on Metal Oxides Using Coumarin as a Probe, ChemCatChem. 11 (2019) 5435–5438. https://doi.org/10.1002/cctc.201901316.

[23] C.M. Lousada, M. Jonsson, Kinetics, Mechanism, and Activation Energy of H_2O_2 Decomposition on the Surface of ZrO_2, J. Phys. Chem. C. 114 (2010) 11202–11208. https://doi.org/10.1021/jp1028933.

[24] E. Ekeroth, M. Jonsson, Oxidation of UO2 by radiolytic oxidants, J. Nucl. Mater. 322 (2003) 242–248. https://doi.org/10.1016/j.jnucmat.2003.07.001.

[25] N.L. Hansson, M. Jonsson, C. Ekberg, K. Spahiu, Modelling radiation-induced oxidative dissolution of UO2-based spent nuclear fuel on the basis of the hydroxyl radical mediated surface mechanism, J. Nucl. Mater. 578 (2023) 154369. https://doi.org/10.1016/j.jnucmat.2023.154369.

[26] J.-Y. Piquemal, E. Briot, J.-M. Brégeault, Preparation of materials in the presence of hydrogen peroxide: from discrete or “zero-dimensional” objects to bulk materials, Dalton Trans. 42 (2013) 29–45. https://doi.org/10.1039/C2DT31660A.

[27] L.E. Eary, L.M. Cathles, A Kinetic Model of UO2 Dissolution in Acid, H202 Solutions That Includes Uranium Peroxide Hydrate Precipitation, Metall. Trans. B. 14 (1983) 325–334.

[28] S.I. Nikitenko, M. Virot, P. Moisy, Sonochemistry of actinides: from ions to nanoparticles and beyond, Radiochim. Acta. 110 (2022) 453–470. https://doi.org/10.1515/ract-2021-1142.

[29] E. Dalodière, M. Virot, V. Morosini, T. Chave, T. Dumas, C. Hennig, T. Wiss, O. Dieste Blanco, D.K. Shuh, T. Tyliszcak, L. Venault, P. Moisy, S.I. Nikitenko, Insights into the sonochemical synthesis and properties of salt-free intrinsic plutonium colloids, Sci. Rep. 7 (2017) 43514. https://doi.org/10.1038/srep43514.

[30] M. Virot, S. Szenknect, T. Chave, N. Dacheux, P. Moisy, S.I. Nikitenko, Uranium carbide dissolution in nitric solution: Sonication vs. silent conditions, J. Nucl. Mater. 441 (2013) 421–430. https://doi.org/10.1016/j.jnucmat.2013.06.021.

[31] Pankaj, M. Ashokkumar, eds., Theoretical and Experimental Sonochemistry Involving Inorganic Systems, Springer Netherlands, Dordrecht, 2011. https://doi.org/10.1007/978-90-481-3887-6.

[32] T.J. Mason, J.P. Lorimer, Applied Sonochemistry, Wiley-VCH Verlag GmbH & Co. KGaA, Weinheim, FRG, 2002. https://doi.org/10.1002/352760054X.

[33] K. Yasui, T. Tuziuti, M. Sivakumar, Y. Iida, Theoretical study of single-bubble sonochemistry, J. Chem. Phys. 122 (2005) 224706. https://doi.org/10.1063/1.1925607.

[34] R. Pflieger, T. Chave, G. Vite, L. Jouve, S.I. Nikitenko, Effect of operational conditions on sonoluminescence and kinetics of H2O2 formation during the sonolysis of water in the presence of Ar/O2 gas mixture, Ultrason. Sonochem. 26 (2015) 169–175. https://doi.org/10.1016/j.ultsonch.2015.02.005.

[35] I. Akhatov, O. Lindau, A. Topolnikov, R. Mettin, N. Vakhitova, W. Lauterborn, Collapse and rebound of a laser-induced cavitation bubble, Phys. Fluids. 13 (2001) 2805–2819. https://doi.org/10.1063/1.1401810.

[36] K.S. Suslick, Mechanochemistry and sonochemistry: concluding remarks, Faraday Discuss. 170 (2014) 411–422. https://doi.org/10.1039/C4FD00148F.
[37] A. Priyadarshi, M. Khavari, T. Subroto, P. Prentice, K. Pericleous, D. Eskin, J. Durodola, I. Tzanakis, Mechanisms of ultrasonic de-agglomeration of oxides through in-situ high-speed observations and acoustic measurements, Ultrason. Sonochem. 79 (2021) 105792. https://doi.org/10.1016/j.ultsonch.2021.105792.
[38] M. Cot-Auriol, M. Virot, C. Micheau, T. Dumas, X. Le Goff, C. Den Auwer, O. Diat, P. Moisy, S.I. Nikitenko, Ultrasonically assisted conversion of uranium trioxide into uranium(VI) intrinsic colloids, Dalton Trans. 50 (2021) 11498–11511. https://doi.org/10.1039/D1DT01609A.
[39] M. Cot-Auriol, M. Virot, T. Dumas, O. Diat, X. Le Goff, P. Moisy, S.I. Nikitenko, Ultrasonically controlled synthesis of UO_{2+x} colloidal nanoparticles, Dalton Trans. 52 (2023) 2135–2144. https://doi.org/10.1039/D2DT03721A.
[40] L. Bonato, M. Virot, X. Le Goff, P. Moisy, S.I. Nikitenko, Sonochemical dissolution of nanoscale ThO_2 and partial conversion into a thorium peroxo sulfate, Ultrason. Sonochem. 69 (2020) 105235. https://doi.org/10.1016/j.ultsonch.2020.105235.
[41] L. Bonato, M. Virot, T. Dumas, A. Mesbah, P. Lecante, D. Prieur, X. Le Goff, C. Hennig, N. Dacheux, P. Moisy, S.I. Nikitenko, Deciphering the Crystal Structure of a Scarce 1D Polymeric Thorium Peroxo Sulfate, Chem. – Eur. J. 25 (2019) 9580–9585. https://doi.org/10.1002/chem.201901426.
[42] J. Martinez, N. Clavier, T. Ducasse, A. Mesbah, F. Audubert, B. Corso, N. Vigier, N. Dacheux, From uranium(IV) oxalate to sintered UO 2 : Consequences of the powders' thermal history on the microstructure, J. Eur. Ceram. Soc. 35 (2015) 4535–4546. https://doi.org/10.1016/j.jeurceramsoc.2015.07.010.
[43] P.N.T. Wells, M.A. Bullen, D.H. Follett, H.F. Freundlich, J.A. James, The dosimetry of small ultrasonic beams, Ultrasonics. 1(2) (1963) 106–110.
[44] D.W. O'Sullivan, M. Tyree, The kinetics of complex formation between Ti(IV) and hydrogen peroxide, Int. J. Chem. Kinet. 39 (2007) 457–461. https://doi.org/10.1002/kin.20259.
[45] R. Ji, M. Virot, R. Pflieger, S.I. Nikitenko, Sonochemical decontamination of magnesium and magnesium-zirconium alloys in mild conditions, J. Hazard. Mater. 406 (2021) 124734. https://doi.org/10.1016/j.jhazmat.2020.124734.
[46] M. Debure, Study of the dissolution of borosilicate glasses in the presence of model magnesian minerals representative of the minerals of the Callovo-Oxfordian clay, MINES ParisTech, 2012.
[47] I. Casas, J. de Pablo, J. Giménez, M.E. Torrero, J. Bruno, E. Cera, R.J. Finch, R.C. Ewing, The role of pe, pH, and carbonate on the solubility of UO2 and uraninite under nominally reducing conditions, Geochim. Cosmochim. Acta. 62 (1998) 2223–2231. https://doi.org/10.1016/S0016-7037(98)00140-9.
[48] F. Clarens, J. de Pablo, I. Casas, J. Giménez, M. Rovira, J. Merino, E. Cera, J. Bruno, J. Quiñones, A. Martínez-Esparza, The oxidative dissolution of unirradiated UO2 by hydrogen peroxide as a function of pH, J. Nucl. Mater. 345 (2005) 225–231. https://doi.org/10.1016/j.jnucmat.2005.06.002.
[49] Ph. Moisy, S.I. Nikitenko, L. Venault, C. Madie, Sonochemical Dissolution of Metallic Plutonium in a Mixture of Nitric and Formic Acid, Ract. 75 (1996) 219–226. https://doi.org/10.1524/ract.1996.75.4.219.
[50] V. Morosini, T. Chave, M. Virot, P. Moisy, S.I. Nikitenko, Sonochemical water splitting in the presence of powdered metal oxides, Ultrason. Sonochem. 29 (2016) 512–516. https://doi.org/10.1016/j.ultsonch.2015.11.006.
[51] F.B. Baker, T.W. Newton, The reaction between uranium(IV) and hydrogen peroxide, J. Phys. Chem. 65 (1961) 1897–1899. https://doi.org/10.1021/j100827a504.
[52] M. Magnin, C. Jégou, R. Caraballo, V. Broudic, M. Tribet, S. Peuget, Z. Talip, Oxidizing dissolution mechanism of an irradiated MOX fuel in underwater aerated conditions at slightly acidic pH, J. Nucl. Mater. 462 (2015) 230–241. https://doi.org/10.1016/j.jnucmat.2015.03.029.

[53] C. Corbel, G. Sattonnay, S. Guilbert, F. Garrido, M.-F. Barthe, C. Jegou, Addition versus radiolytic production effects of hydrogen peroxide on aqueous corrosion of UO_2, J. Nucl. Mater. 348 (2006) 1–17. https://doi.org/10.1016/j.jnucmat.2005.05.009.
[54] K.-A.H. Kubatko, K.B. Helean, A. Navrotsky, P.C. Burns, Stability of Peroxide-Containing Uranyl Minerals, Science. 302 (2003) 1191–1193. https://doi.org/10.1126/science.1090259.
[55] S. Bastians, G. Crump, W.P. Griffith, R. Withnall, Raspite and studtite: Raman spectra of two unique minerals, J. Raman Spectrosc. 35 (2004) 726–731. https://doi.org/10.1002/jrs.1176.
[56] P.F. Weck, E. Kim, Uncloaking the Thermodynamics of the Studtite to Metastudtite Shear-Induced Transformation, J. Phys. Chem. C. 120 (2016) 16553–16560. https://doi.org/10.1021/acs.jpcc.6b05967.
[57] M.L. Schlegel, C. Jegou, Uraninite alteration by H2O2 solutions and formation of secondary phases: An in situ microRaman spectroscopy and synchrotron X-ray diffraction study, J. Nucl. Mater. 572 (2022) 154056. https://doi.org/10.1016/j.jnucmat.2022.154056.
[58] E. Dalodière, M. Virot, P. Moisy, S.I. Nikitenko, Effect of ultrasonic frequency on H2O2 sonochemical formation rate in aqueous nitric acid solutions in the presence of oxygen, Ultrason. Sonochem. 29 (2016) 198–204. https://doi.org/10.1016/j.ultsonch.2015.09.014.
[59] L. Venault, Ph. Moisy, S.I. Nikitenko, C. Madic, Kinetics of nitrous acid formation in nitric acid solutions under the effect of power ultrasound, Ultrason. Sonochem. 4 (1997) 195–204. https://doi.org/10.1016/S1350-4177(97)00010-2.
[60] I. Tzanakis, W.W. Xu, D.G. Eskin, P.D. Lee, N. Kotsovinos, In situ observation and analysis of ultrasonic capillary effect in molten aluminium, Ultrason. Sonochem. 27 (2015) 72–80. https://doi.org/10.1016/j.ultsonch.2015.04.029.
[61] D. Nikolai, D. Valerio, Physical Backgrounds for Application of Power Ultrasound in Fluorescent Dye Penetrant Inspection, in: Budapest, 2005.
[62] N. Dezhkunov, A. Francescutto, P. Ciuti, P. Ignatenko, Ultrasonic capillary effect and sonoluminescence, in: Paris, 2003: p. 4.
[63] N.V. Dezhkunov, P.P. Prokhorenko, Action of ultrasound on the rise of a liquid in a capillary tube and its dependence on the properties of the liquid, J. Eng. Phys. 39 (1979) 1014–1019. https://doi.org/10.1007/BF00825930.
[64] N. Malykh, V.M. Petrov, G. Sankin, On Sonocapillary Effect, in: Paris, 2003: p. 4.
[65] R. Kusaka, Y. Kumagai, T. Yomogida, M. Takano, M. Watanabe, T. Sasaki, D. Akiyama, N. Sato, A. Kirishima, Distribution of studtite and metastudtite generated on the surface of U_3O_8: application of Raman imaging technique to uranium compound, J. Nucl. Sci. Technol. 58 (2021) 629–634. https://doi.org/10.1080/00223131.2020.1854881.
[66] B.D. Anderson, J.B. Tracy, Nanoparticle conversion chemistry: Kirkendall effect, galvanic exchange, and anion exchange, Nanoscale. 6 (2014) 12195–12216. https://doi.org/10.1039/C4NR02025A.
[67] N. Friedl, F.G. Rammerstorfer, F.D. Fischer, Buckling of stretched strips, Comput. Struct. 78 (2000) 185–190. https://doi.org/10.1016/S0045-7949(00)00072-9.
[68] F.G. Rammerstorfer, Buckling of elastic structures under tensile loads, Acta Mech. 229 (2018) 881–900. https://doi.org/10.1007/s00707-017-2006-1.
[69] A. Brotchie, F. Grieser, M. Ashokkumar, Effect of Power and Frequency on Bubble-Size Distributions in Acoustic Cavitation, Phys. Rev. Lett. 102 (2009) 084302. https://doi.org/10.1103/PhysRevLett.102.084302.
[70] I. Tzanakis, D.G. Eskin, A. Georgoulas, D.K. Fytanidis, Incubation pit analysis and calculation of the hydrodynamic impact pressure from the implosion of an acoustic cavitation bubble, Ultrason. Sonochem. 21 (2014) 866–878. https://doi.org/10.1016/j.ultsonch.2013.10.003.
[71] W. Bai, P. Hébraud, M. Ashokkumar, Y. Hemar, Investigation on the pitting of potato starch granules during high frequency ultrasound treatment, Ultrason. Sonochem. 35 (2017) 547–555. https://doi.org/10.1016/j.ultsonch.2016.05.022.
[72] F. Sugino, K. Yamamoto, Mechanism for ultrasonic pitting of starch particles, Jpn. J. Appl. Phys. 60 (2021) SDDD08. https://doi.org/10.35848/1347-4065/abef09.

[73] A. Inui, A. Honda, S. Yamanaka, T. Ikeno, K. Yamamoto, Effect of ultrasonic frequency and surfactant addition on microcapsule destruction, Ultrason. Sonochem. 70 (2021) 105308. https://doi.org/10.1016/j.ultsonch.2020.105308.
[74] E.D. Andrews, D.F. Rivas, I.R. Peters, Cavity collapse near slot geometries, J. Fluid Mech. 901 (2020) A29. https://doi.org/10.1017/jfm.2020.552.
[75] M. Koch, J.M. Rosselló, C. Lechner, W. Lauterborn, R. Mettin, Dynamics of a Laser-Induced Bubble above the Flat Top of a Solid Cylinder—Mushroom-Shaped Bubbles and the Fast Jet, Fluids. 7 (2021) 2. https://doi.org/10.3390/fluids7010002.